Resilience-Oriented Restoration of Coupled Power and Water Distribution Systems via Coordinated Demand Response and Hydraulic Flexibility

Mohsen Foroughifard[1], Amir Abdollahi[1,*], Masoud Rashidinejad[1], Ali Yazhari Kermani[1] and Mahdi Ramezani[1]

[1]*Department of Electrical Engineering, Shahid Bahonar University of Kerman, Kerman, Iran*
**Corresponding author: a.abdollahi@uk.ac.ir*

Manuscript received 05 July, 2026; revised 23 July, 2026; accepted 10 August, 2026. Paper no. JEMT-2607-1607.

The increasing frequency of high-impact, low-probability (HILP) events poses a serious threat to modern distribution systems, motivating a shift from robustness toward resilience-oriented operation. In urban lifeline systems, the power distribution system (PDS) and the water distribution system (WDS) are tightly interdependent, since water pumping is energy-intensive and any power outage propagates directly into water shortages. Restoration strategies that treat the two networks separately therefore overlook important coordination opportunities and may allocate scarce resources inefficiently. Most existing models address either the electrical reconfiguration of the power network or the hydraulic operation of the water network and rarely incorporate comprehensive demand response (DR). This paper proposes a fully linearized mixed-integer linear programming (MILP) framework for the resilience-oriented restoration of coupled PDS and WDS. The operational constraints of both infrastructures, including network reconfiguration; distributed energy resource (DER) dispatch (including gas-fired distributed generators (DGs), photovoltaic (PV) units, and electrical energy storages (EESs)); hydraulic head losses; variable-speed pump dynamics; and tank storage, are embedded within a single model and coordinated through nexus constraints together with three DR programs. The nonlinearities of the Hazen–Williams equation and the pump characteristics are systematically linearized to preserve tractability. The framework is evaluated on a coupled IEEE 33-bus power system and a 15-node water network under a severe fault scenario. The results reveal that hydraulic flexibility is the dominant restoration mechanism, while DR provides a complementary improvement, and their coordinated use delivers the most effective recovery of both infrastructures.

Keywords: *Coupled power and water distribution systems, Demand response, Hydraulic flexibility, Mixed-integer linear programming, Resilience-oriented restoration*

http://dx.doi.org/10.22109/jemt.2026.590262.1607

Nomenclature

Indices

d	Index of gas-fired DG units
e	Index of energy storage units
i,j	Indices of PDS nodes
k	Index of water storage tanks
l	Index of power lines or water pipes
m,n	Indices of WDS nodes
p	Index of photovoltaic units
r	Index of pump discrete speed levels
t	Index of time periods
τ	Index of time delay for transferable loads

Sets

$\mathcal{B}$	Set of power distribution buses
$\mathcal{B}^{DR}$	Set of buses participating in DR programs
$\mathcal{B}^{source}$	Set of buses with generation capability (DG, PV, EES, substation)
$\mathcal{L}$	Set of power distribution lines
$\mathcal{L}_i$	Set of power lines incident to bus i
$\mathcal{L}^W$	Set of water distribution pipes
$\mathcal{N}$	Set of water distribution nodes
$\mathcal{G}$	Set of gas-fired DGs
$\mathcal{E}$	Set of energy storage units
$\mathcal{P}$	Set of photovoltaic units
$\mathcal{K}$	Set of water storage tanks

$\mathcal{P}^{pump}$	Set of water pumps
$\mathcal{T}$	Set of time periods
$\mathcal{P}_n^{in}$	Set of pumps entering node n
$\mathcal{P}_n^{out}$	Set of pumps leaving node n
$\mathcal{L}_n^{W,in}$	Set of pipes entering node n
$\mathcal{L}_n^{W,out}$	Set of pipes leaving node n

Parameters

$A_k^{surface}, H_k^{base}$	Surface area (m²) and base head (m) of tank k
A_r	Pump head coefficient at speed level r (m)
B_r	Pump head loss coefficient at speed level r
C_r	Pump power constant coefficient at speed level r (p.u.)
D_r	Pump power flow coefficient at speed level r
DG_d^{max}	Maximum active power output of DG d (p.u.)
$DR_{frac}(i)$	Maximum fraction of load that can be shifted at bus i
$DR_{cur}(i)$	Maximum fraction of load that can be curtailed at bus i
$DR_{tra}(i)$	Maximum fraction of load that can be transferred at bus i
$E_e^{max}, E_e^{init}, \eta_{ch}, \eta_{dis}$	Storage capacity (p.u.), initial SOC, charging/discharging efficiencies
f_l	Hazen-Williams loss coefficient for pipe l
H_n^{min}, H_n^{max}	Min/max hydraulic head at node n (m)
K, R	Number of linearization segments and pump speed levels
M	Big-M constant
N^L, N^P, N^W	Number of power lines, power buses, water nodes
$P_{i,t}^D, Q_{i,t}^D$	Active and reactive power demand at bus i (p.u.)
$\bar{P}_l, \bar{Q}_l$	Max active/reactive power flow on line l (p.u.)
$\bar{P}_e^{ch}, \bar{P}_e^{dis}$	Max charge/discharge rate of storage e (p.u.)
PV_p^{max}	Maximum active power output of PV unit p (p.u.)
$Profile_{p,t}^{PV}$	Solar irradiance profile for PV unit p at time t
$\bar{P}_p^{pump}, \bar{Q}_p^{pump}$	Max pump power (p.u.) and max water flow (m³/h)
$\bar{Q}_k^{tank,in}, \bar{Q}_k^{tank,out}$	Max tank inflow/outflow (m³/h)
$\bar{Q}_l^W$	Max water flow in pipe l (m³/h)
R_l, X_l	Resistance and reactance of power line l (p.u.)
V_k^{min}, V_k^{max}	Min/max tank volume (m³)
V_{min}, V_{max}	Min/max squared voltage magnitude (p.u.²)
$W_{n,t}^D$	Water demand at node n (m³/h)
λ, τ_{max}	RI weight for PDS and max transfer window
$\phi_{DG}, \phi_{load}, \phi_i$	Power factor angles of DG, load, and bus i
ω_i^P, ω_n^W	Priority weights for electric load at bus i and water demand at node n
Ω_r	Pump speed at level r (p.u.)

Variables

$E_{e,t}$	State of charge of storage e (p.u.)
$H_{n,t}$	Hydraulic head at node n (m)
$P_{d,t}^{DG}, P_{p,t}^{PV}$	DG and PV power outputs (p.u.)
$P_{e,t}^{ch}, P_{e,t}^{dis}$	Charge and discharge power of storage e (p.u.)
$P_{l,t}, Q_{l,t}$	Active and reactive power flow on power line l (p.u.)
$P_{p,t}^{pump}, Q_{p,t}^{pump}$	Pump power consumption (p.u.) and water flow (m³/h)
$P_{i,t}^{load,eff}, Q_{i,t}^{load,eff}$	Effective active/reactive load at bus i (p.u.)
$P_{i,t}^{shift,up/dn}$	Shiftable load increase/decrease at bus i (p.u.)
$P_{i,t}^{cur,up/dn}$	Curtailable load rebound/reduction at bus i (p.u.)
$P_{i,t}^{tra,up/dn}$	Transferable load increase/decrease at bus i (p.u.)
$Q_{l,t}^W$	Water flow in pipe l (m³/h)
$Q_{n,t}^{source}$	Water injection from source at node n (m³/h)
$Q_{k,t}^{tank,in/out}$	Tank inflow/outflow (m³/h)
$Q_{l,k,t}^{seg}$	Segmented water flow in pipe l, segment k (m³/h)
$Q_{p,t,r}^{lin}$	Linearization variable for pump p, speed r (m³/h)
$V_{k,t}$	Volume of tank k (m³)
f_l	Artificial flow on power line l for radiality
$root_i, x_i, z_l$	Binary: root bus, energized bus, closed power line
$\gamma_{i,t}^P$	Fraction of electric demand served at bus i
$\gamma_{n,t}^W$	Fraction of water demand served at node n
$\delta_{i,t}^{cur}, \delta_{i,t}^{tra}$	Binary: curtailment/transfer applied at bus i
$\delta_{p,t,r}^{pump}, \chi_{p,t}^{pump}$	Binary: speed selected, pump on
$v_{i,t}$	Squared voltage magnitude at bus i (p.u.²)
RI, R_{PDS}, R_{WDS}	Composite resilience indices

1. Introduction

1.1. Motivation and Background

Recent advances in climate data modeling have shown that extreme weather events are becoming more frequent and more severe [1]. HILP events are rare, catastrophic, and unpredictable events without historical precedents that can trigger cascading failures in interconnected systems [2]. The changing threat landscape suggests the approach to dealing with critical infrastructure should be shifted from robustness to resilience, using a broader and more dynamic paradigm. Resilience is the system's ability to anticipate HILP events, resist them, and restore services quickly after a disruption [3]. Moreover, resilience is described as a dynamic process, which is grounded on three fundamental pillars: the ability to absorb disruptive shocks, the capacity to adapt to changing conditions, and the effectiveness in returning to a stable operational regime [4]. These resilience principles are universally applicable to critical infrastructure systems, but they are particularly vital for modern PDS. Because of their inherent vulnerability to cascading failures due to extreme weather events, PDSs often experience extensive infrastructure damage and long power outages [5]. Finally, the importance of proper management of these HILP events is highlighted, since their severe physical and operational impacts reveal critical grid vulnerabilities and lead to significant economic losses [6].

Addressing these critical vulnerabilities is considered to provide direct guidance for the primary operational objective in the post-disaster restoration phase: maximizing the recovery of critical loads. The primary goal in the post-disaster restoration phase is defined as the recovery of critical loads to the maximum extent possible by employing tactical actions such as network reconfiguration to isolate damaged regions, optimal rescheduling of DERs for local stability, and DR programs to match limited supply with critical demand [7], [8]. However, the implementation of these tactical actions, such as reconfiguration, DER dispatch, and DR, in a coordinated and optimal manner in large-scale networks is recognized as highly complex. This complexity points to the urgency of developing systematic and quantifiable frameworks to guide restoration efforts effectively. Climate trends are expected to further increase the frequency of such HILP conditions; thus, systematic and quantifiable frameworks for restoration are critical to the protection of the structural and functional integrity of urban lifeline systems [9]. In this context, the interdependence between the PDS and the WDS adds another layer of complexity, as power outages directly disrupt energy-intensive water treatment and pumping, cascading into severe water shortages that compound the societal impacts of extreme events. Hence, recovery strategies should go beyond isolated PDS restoration and explicitly incorporate the coordinated operation of water storage, pumping facilities, and demand-side management in the WDS together with grid reconfiguration and DER scheduling to ensure the restoration efforts meet the needs of both infrastructures simultaneously [10].

Beyond restoration, the broader sustainability of coupled energy–water systems is being pursued along several complementary directions, such as the renewable provision of hot-water demand through solar-thermal systems [11], energy-free freshwater sources like urban fog-water harvesting that reduce the energy burden of water supply [12], and the growing use of artificial intelligence for fault detection, performance optimization, and water-energy nexus management [13]. While these directions target long-term sustainability rather than post-disaster recovery, they underline the increasingly tight coupling of energy and water systems that motivates the present study.

1.2. Literature review

The increasing need for resilience-oriented approaches has led to extensive research efforts aiming to enhance post-disaster restoration strategies. Initially, many of these studies focused solely on the independent recovery of PDS. In this context, distribution system reconfiguration (DSR), the formation of microgrids, and the integration of distributed energy resources (DERs) have been proposed as efficient solutions for the restoration of critical loads during islanded operation after grid interruption [14], [15], [16], [17]. According to research, the use of local resources in the form of microgrids can substantially improve the effectiveness of the restoration [8], [18]. In addition to operational measures, preventive planning such as line hardening, emergency generator allocation, and optimal placement of automated switches has been investigated to mitigate the destructive impacts of outages and to facilitate DSR operations [18], [19], [20], [21].

Even with these improvements, focusing only on the separate management of PDSs during emergencies ignores how outages can affect other critical infrastructures that depend on them, especially WDSs. Such an approach can lead to poor resource allocation [22], [23]. To tackle this challenge, recent studies have focused on modeling the interdependency between PDS and WDS in the restoration horizon [10], [24], [25]. The studies have demonstrated that the finite capacity of the electrical grid can be coordinated with pumping stations by exploiting the inherent flexibility of WDSs, like storage tanks [26]. Such a strategy can reduce water supply interruptions to consumers and relieve load on the pumps from the power grid during critical hours, which in turn releases available capacity to support other critical PDS loads [24], [27].

Besides supply-side and grid coordination, demand-side management (DSM) can be a complementary restoration strategy. For this purpose, DR programs have been applied as effective tools to maintain power balance within microgrids and emergency conditions [28]. Beyond the electricity sector alone, integrated DR spanning multiple energy carriers has also been shown to provide substantial flexibility, for instance by coordinating electricity and natural gas DR within a flexibility-based scheduling framework [29]. Flexible loads help the grid to overcome generation shortfalls due to equipment failures through load shifting, shedding, or rescheduling [8], [30]. In a similar manner, energy storage systems have been established as key flexible resources in system operation, where their fast response complements demand-side elasticity in managing uncertainty [31]. In this regard, water network facilities, due to their high energy consumption, possess significant potential for participating in DR programs [32]. Integrating the energy flexibility of water networks within the framework of energy hubs not only reduces operational expenses under normal conditions but also enhances the survivability and resilience of the integrated system against unexpected blackouts [33].

Recent studies have explored resilience in different contexts. In [34], a model-based framework was developed to assess the resilience of water resource recovery facilities against power outages, while a genetic-algorithm-based restoration method incorporating probabilistic circuit-breaker models was proposed for power systems after storm-induced failures [35]. For microgrids, a convex optimization model was presented for resilience-oriented operation under both grid-connected and isolated conditions [36], and the economic operation of energy hubs was examined using resilience and energy-security indices that distinguish critical from non-critical loads [37]. More recently, transient hydraulic dynamics and spatio-temporal cascading failures were incorporated into coupled power-water restoration through an offline deep reinforcement learning approach [38]; although effective for rapid, learning-based decision-making, that approach does not guarantee global optimality and does not exploit DR or tank flexibility as coordinated restoration resources.

Taken together, these studies reveal a critical gap that can be described along three lines. First, most restoration models for interdependent networks either overlook the potential of comprehensive DR programs, or, when DR is considered, capture only one side of the coupled problem, addressing either the hydraulic constraints of the water network or the electrical reconfiguration of the PDS, but rarely both within a single formulation. Second, models that do address the power–water interdependency typically rely on simplified or decoupled hydraulic representations, and a detailed operational model of the water network that captures Hazen–Williams head losses, variable-speed pump behavior, and tank dynamics is rarely embedded together with the electrical restoration problem in one optimization. Third, most coupled formulations retain nonlinear or non-convex terms and are therefore solved by heuristic, metaheuristic, or learning-based algorithms that cannot guarantee global optimality, and the joint role of DR and hydraulic storage as complementary flexibility mechanisms has not been quantitatively isolated. As summarized in Table 1, none of the existing models simultaneously incorporate all these components. To bridge this gap, this paper proposes a quantitative and integrated framework for the resilience-oriented restoration of interdependent power and water distribution systems, in which all hydraulic and pump nonlinearities are linearized so that the problem is cast as a MILP solvable to a certified optimality gap, and DR capacities are optimized in coordination with grid reconfiguration and the dispatch of DERs.

Table 1. Comprehensive Literature Review Comparison

Ref.	[8]	[10]	[14]	[15]	[16]	[24]	[32]	[34]	[35]	[36]	[37]	[38]	This Paper
Year	2022	2024	2021	2019	2022	2021	2019	2021	2025	2025	2024	2026	2026
WDS	✗	✓	✗	✗	✗	✓	✓	✓	✗	✗	✗	✓	✓
DR Programs	✓	✗	✗	✗	✗	✗	✓	✗	✗	✗	✗	✗	✓
DERs & EES Integration	✓	✓	✗	✓	✓	✓	✗	✗	✓	✓	✓	✗	✓
Tie Lines	✓	✗	✓	✓	✓	✓	✗	✗	✗	✓	✗	✓	✓
MILP Structure	✓	✗	✓	✓	✓	✗	✓	✗	✗	✓	✓	✓	✓
Reconfiguration	✓	✗	✓	✓	✓	✓	✗	✗	✓	✓	✗	✓	✓
Resilience-Oriented	✓	✓	✓	✓	✓	✓	✗	✓	✓	✓	✓	✓	✓

1.3. Contributions

To the best of the authors' knowledge, no prior work has embedded power network reconfiguration, hydraulic dynamics, and comprehensive DR programs within a fully linearized MILP framework for the coordinated restoration of interdependent PDS and WDS. To realize this goal, this paper proposes an integrated restoration framework for coupled PDS and WDS, where the operational constraints of both infrastructures, including hydraulic head losses, variable-speed pump dynamics, tank storage, and three types of DR programs, are incorporated within a single optimization model. The nonlinearities arising from the Hazen-Williams equation and pump characteristics are systematically linearized using piecewise linear approximation, discrete speed selection, and the big-M method, yielding a computationally tractable MILP formulation solvable to global optimality. The two systems are interconnected via nexus constraints, where pump power consumption is modeled as an electrical load and water storage in tanks offers hydraulic flexibility. The composite resilience index (RI) is proposed as a weighted sum of the restoration of electric and water loads. The main contributions of this paper are summarized below.

- A fully linearized MILP framework is developed to coordinate the restoration of interdependent PDS and WDS within a single optimization model.
- The detailed hydraulic model formulation includes piecewise linearization of the Hazen-Williams equation, discrete speed pump modeling and tank head-volume dynamics.
- Demand-side flexibility is captured through an advanced DR scheme with shiftable, curtailable and transferable loads with rebound effects.
- Nexus constraints explicitly model the interdependency between PDS and WDS, such that restoration decisions consider the mutual impacts of both systems.

1.4. Paper structure

The remainder of this paper is organized as follows. Section 2 presents the formulation of the proposed MILP model, including the operational constraints of the PDS, the WDS, their interdependencies, and the linearization techniques employed to convert the nonlinear hydraulic constraints into a linearized framework. Section 3 provides the numerical results and discussions from case studies conducted on a coupled IEEE 33-bus PDS and a 15-node WDS. Finally, Section 4 provides the conclusion and outlines directions for future research.

2. Mathematical Formulation

The overall framework of the resilience-oriented restoration for coupled PDS and WDSs is illustrated in Fig. 1 and formulated as a MILP model. The proposed formulation models the operational constraints of each subsystem separately, while the interdependency between the two is modeled through coupling constraints that explicitly account for the electrical power consumption of water pumps and the hydraulic flexibility provided by water storage tanks. Optimization is performed over a 24-hour horizon.

The PDS model includes radial topology constraints, linearized DistFlow voltage-drop equations, DER dispatch (including DGs, PV units, and EESs), and three types of DR programs, i.e., shiftable, curtailable, and transferable loads with recovery dynamics. The hydraulic model of the WDS consists of mass conservation at each node, Hazen-Williams head losses in pipes, variable-speed pump operation with discrete speed selection, and tank head-volume dynamics. All nonlinearities are systematically linearized with a piecewise linear approximation and the big-M method, resulting in a fully linearized MILP formulation that can be solved to global optimality. The objective is to maximize a composite Resilience Index (RI), defined as the weighted sum of electric load restoration, and water demand restoration to achieve balanced and coordinated recovery of both critical infrastructures.

The remainder of this section is organized as follows. Section 2.1 presents the objective function, where the composite resilience index is formulated as a weighted combination of electric and water restoration indices. Section 2.2 provides the detailed mathematical formulation of the constraints for the PDS, including radial topology enforcement, linearized DistFlow voltage equations, dispatch of distributed energy resources, and the three types of demand response programs. Section 2.3 describes the constraints of the WDS: mass conservation, pipe head losses, modeling of variable speed pumps, and tank dynamics. Finally, Section 2.4 presents the coupling constraints that link the two subsystems through the pump power consumption and the associated reactive power requirements, yielding a genuinely coordinated restoration strategy.

2.1. Objective Function

The primary objective of the proposed restoration framework is to maximize the overall resilience of the coupled power and water distribution systems over the restoration horizon. To this end, a composite Resilience Index (RI) is defined as the weighted sum of the normalized electric load restoration and water demand restoration, ensuring a balanced recovery of both critical infrastructures. This formulation follows the resilience metric proposed in [39] for interdependent infrastructure networks, where system performance is measured as the ratio of weighted served demand to weighted total demand over the restoration horizon. The objective function is formulated as follows.

$$Maximize\ RI = \lambda \cdot R_{PDS} + (1-\lambda) \cdot R_{WDS} \quad (1)$$

where λ is a number between zero and one that shows how important it is to restore electric service compared to water service. The value of λ can also be changed by the system operator depending on the priorities of the affected community, criticality of electric loads, and urgency of restoring the water supply. In this case, λ is set to 0.6, which is a compromise between the two objectives, with a slightly higher weight on the restoration of the electric load, but still with a significant weight on the recovery of the water supply.

The electric load restoration index quantifies the fraction of the total weighted electric demand that is successfully served during the restoration horizon. It is defined as the ratio of the weighted served energy to the weighted total demand over all PDS buses, and time intervals as expressed in Eq. (2). The numerator of this expression is the total weighted energy actually delivered to customers, where each bus load is multiplied by its priority weight and the fraction of demand served. The denominator is the total weighted energy needed to serve all loads completely. Critical facilities (e.g., hospitals, emergency response centers) are assigned higher weights to prioritize their restoration.

$$R_{PDS} = \frac{\sum_{t=1}^{T} \sum_{i=1}^{N^P} \omega_i^P \cdot P_{i,t}^D \cdot \gamma_{i,t}^P}{\sum_{t=1}^{T} \sum_{i=1}^{N^P} \omega_i^P \cdot P_{i,t}^D} \quad (2)$$

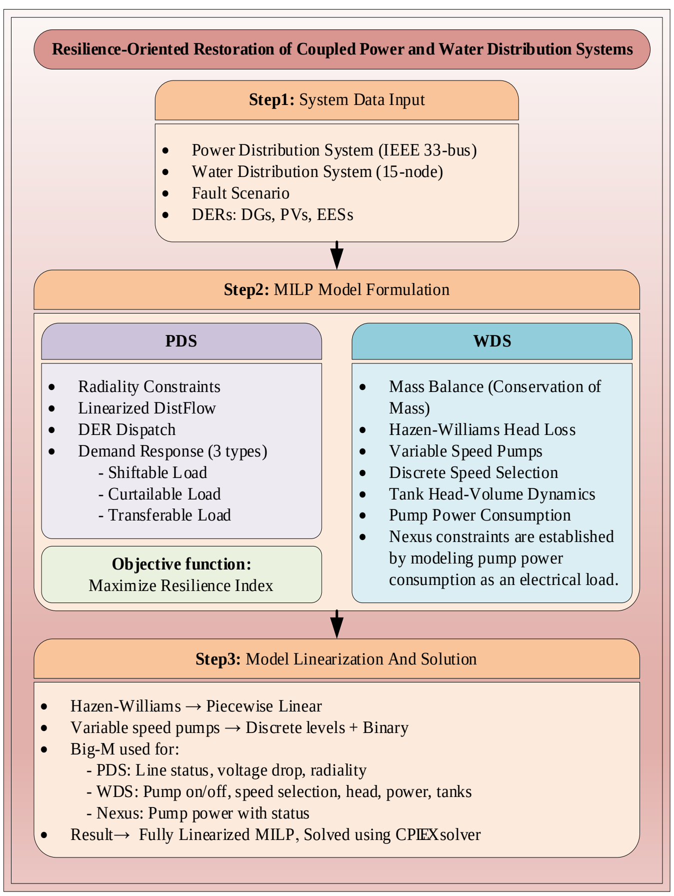

Fig. 1. Overview of the proposed resilience-oriented restoration of coupled power and water distribution systems

Also, the water demand restoration index is the proportion of the total weighted water demand that is successfully delivered to consumers. It is expressed as the ratio of the weighted delivered water volume to the weighted total water demand over all WDS nodes, and time steps in Eq. (3). In this study, the water demands are all equally weighted to avoid artificial prioritization and to allow the hydraulic network's physical constraints to determine the optimal water distribution.

$$R_{WDS} = \frac{\sum_{t=1}^{T} \sum_{n=1}^{N^W} \omega_n^W \cdot W_{n,t}^D \cdot \gamma_{n,t}^W}{\sum_{t=1}^{T} \sum_{n=1}^{N^W} \omega_n^W \cdot W_{n,t}^D} \quad (3)$$

2.2. PDS Constraints

The power flow in the PDS is modeled by a linearized DistFlow formulation which captures the steady-state behavior of the radial distribution network. The model considers topology constraints, limits on the voltages, dispatch of distributed energy resources (DGs, PV units and EESs) and three types of DR programs (shiftable, curtailable and transferable) to provide flexibility during restoration.

The artificial flow method is used to impose a radial structure after the reconfiguration [16]. As can be seen from Eq. (4), the number of closed lines has to equal the number of energized buses minus the number of root buses. The artificial flow balance at each bus is given by Eq. (5), where for source buses the term $-M \cdot root_i$ relaxes the constraint when a bus is selected as a root. Artificial flow on open lines is forced to zero by Eq. (6) using a big-M constant. A bus can be energized only if at least one incident line is closed or if it is designated as a root, as stated in Eq. (7). Bus 1 (the main substation) is disconnected in islanded mode and cannot be a root, as given in Eq. (8). Together, these constraints preserve the radial topology of the distribution network after reconfiguration, ensuring that each energized bus is supplied through a single path without forming loops, consistent with standard distribution-system operation.

$$\sum_{l=1}^{N^L} z_l = \sum_{i=1}^{N^P} x_i - \sum_{i=1}^{N^P} root_i \quad (4)$$

$$\sum_{l:to(l)=i} f_l - \sum_{l:from(l)=i} f_l = \begin{cases} x_i, & i \notin \mathcal{B}^{source} \\ x_i - M \cdot root_i, & i \in \mathcal{B}^{source} \end{cases}, \forall i \quad (5)$$

$$| f_l | \le M \cdot z_l, \forall l \quad (6)$$

$$x_i \le \sum_{l \in \mathcal{L}_i} z_l + root_i, \forall i \quad (7)$$

$$x_1 = 0, root_1 = 0 \quad (8)$$

For each line, the linearized voltage drop equations are enforced in Eqs. (9) and (10) when the line is closed, and deactivated using big-M when open. Line power flows are limited by thermal capacity and forced to zero on open lines via Eq. (11). Voltage magnitudes are constrained within permissible limits in Eqs. (12) and (13), with relaxation for de-energized buses [40].

$$v_{j,t} - v_{i,t} + 2(R_l P_{l,t} + X_l Q_{l,t}) \le M(1 - z_l), \forall l, t \quad (9)$$

$$v_{j,t} - v_{i,t} + 2(R_l P_{l,t} + X_l Q_{l,t}) \ge -M(1 - z_l), \forall l, t \quad (10)$$

$$| P_{l,t} | \le \bar{P}_l \cdot z_l, | Q_{l,t} | \le \bar{Q}_l \cdot z_l, \forall l, t \quad (11)$$

$$V_{min} \le v_{i,t} \le V_{max}, \forall i, t \quad (12)$$

$$V_{min} \cdot x_i \le v_{i,t} \le V_{max} \cdot x_i + (1 - x_i), \forall i, t \quad (13)$$

The dispatch of DERs is formulated as follows. Eq. (14) restricts the gas-fired DG output to its rated capacity. The PV generation is limited by the available solar irradiance in Eq. (15). For the EES model, charging and discharging limits are imposed in Eqs. (16)-(17) and the simultaneous charge/discharge is prevented by binary variables in Eq. (18). The state-of-charge dynamics are provided in Eqs. (19)-(20). The capacity constraints of the storage and a minimum final state-of-charge are imposed in Eqs. (21)-(22) [41].

$$0 \le P_{d,t}^{DG} \le DG_d^{max}, \forall d, t \tag{14}$$

$$0 \le P_{p,t}^{PV} \le PV_p^{max} \cdot Profile_{p,t}^{PV}, \forall p, t \tag{15}$$

$$0 \le P_{e,t}^{ch} \le \bar{P}_e^{ch}, \forall e, t \tag{16}$$

$$0 \le P_{e,t}^{dis} \le \bar{P}_e^{dis}, \forall e, t \tag{17}$$

$$u_{e,t}^{ch} + u_{e,t}^{dis} \le 1, \forall e, t \tag{18}$$

$$E_{e,1} = E_e^{init} + \eta_{ch} P_{e,1}^{ch} - \frac{1}{\eta_{dis}} P_{e,1}^{dis}, \forall e \tag{19}$$

$$E_{e,t} = E_{e,t-1} + \eta_{ch} P_{e,t}^{ch} - \frac{1}{\eta_{dis}} P_{e,t}^{dis}, \forall e, t > 1 \tag{20}$$

$$0 \le E_{e,t} \le E_e^{max}, \forall e, t \tag{21}$$

$$E_{e,T} \ge 0.1 \cdot E_e^{max}, \forall e \tag{22}$$

This model includes three types of DR programs, based on the formulations proposed in [8]. Shiftable loads are loads where a part of the electricity consumption can be shifted from peak hours to off-peak hours with the total consumption of energy per day being the same. The net power shift at each bus is defined as the net difference of the upward (increase) and downward (decrease) shifted power in Eq. (23). The amount of load that can be shifted up or down at each hour is limited to a fixed fraction of the base load, as enforced in Eqs. (24) and (25). Eq. (26) forces that the total energy shifted down over the 24-hour horizon must equal the total energy shifted up to conserve energy. This kind of DR is particularly efficient for appliances like washing machines, dishwashers and electric water heaters with the flexibility for the consumer to choose the operating time.

$$P_{i,t}^{shift,net} = P_{i,t}^{shift,up} - P_{i,t}^{shift,dn}, \forall i \in \mathcal{B}^{DR}, t \tag{23}$$

$$0 \le P_{i,t}^{shift,dn} \le DR_{frac}(i) \cdot P_{i,t}^{D}, \forall i \in \mathcal{B}^{DR}, t \tag{24}$$

$$0 \le P_{i,t}^{shift,up} \le DR_{frac}(i) \cdot P_{i,t}^{D}, \forall i \in \mathcal{B}^{DR}, t \tag{25}$$

$$\sum_{t=1}^{T} P_{i,t}^{shift,dn} = \sum_{t=1}^{T} P_{i,t}^{shift,up}, \forall i \in \mathcal{B}^{DR} \tag{26}$$

Curtailable loads allow the system operator to lower power consumption during critical peak periods, with the curtailed energy subsequently restored over the following three hours according to a predetermined rebound pattern. As expressed in Eq. (27), 60% of the curtailed power returns after one hour, 30% after two hours, and the remaining 10% after three hours, so that the total daily energy consumption is preserved. The share of load that may be curtailed in a given hour is capped at a specified fraction of the base demand and governed by a binary variable, as stated in Eq. (28), whereas Eq. (29) bounds the associated rebound power. The binary curtailment status at each bus and time step is defined in Eq. (30). This category of DR is well suited to commercial and residential loads, which can typically tolerate brief interruptions without meaningful operational disruption.

$$P_{i,t}^{cur,up} = 0.6 P_{i,t-1}^{cur,dn} + 0.3 P_{i,t-2}^{cur,dn} + 0.1 P_{i,t-3}^{cur,dn} \\ , \forall i \in \mathcal{B}^{DR}, t \ge 4 \tag{27}$$

$$0 \le P_{i,t}^{cur,dn} \le DR_{cur}(i) \cdot P_{i,t}^{D} \cdot \delta_{i,t}^{cur}, \forall i \in \mathcal{B}^{DR}, t \tag{28}$$

$$0 \le P_{i,t}^{cur,up} \le DR_{cur}(i) \cdot P_{i,t}^{D}, \forall i \in \mathcal{B}^{DR}, t \tag{29}$$

$$\delta_{i,t}^{cur} \in \{0,1\}, \forall i \in \mathcal{B}^{DR}, t \tag{30}$$

Transferable loads allow a consumption block to be moved from one time interval to another later time within a given maximum time window, without interruption once started. This type of DR is suitable for loads such as electric vehicle charging, space heating and industrial processes with fixed durations. The power at the destination hour shifted upward in Eq. (31) is distributed uniformly over the admissible time window. The amount of load that can be transferred down is limited by a pre-defined fraction of the base load and controlled by a binary variable in Eq. (32), while the upward transfer is limited in Eq. (33). Eq. (34) is a binary variable for the application of load transfer or not for each bus and each time. This formulation guarantees that the total daily energy consumption is the same while providing operational flexibility to the system operator.

$$P_{i,t}^{tra,up} = \sum_{\tau=1}^{\tau_{max}} \frac{1}{\tau_{max}} P_{i,t}^{tra,dn}, \forall i \in \mathcal{B}^{DR}, t \tag{31}$$

$$0 \le P_{i,t}^{tra,dn} \le DR_{tra}(i) \cdot P_{i,t}^{D} \cdot \delta_{i,t}^{tra}, \forall i \in \mathcal{B}^{DR}, t \tag{32}$$

$$0 \le P_{i,t}^{tra,up} \le DR_{tra}(i) \cdot P_{i,t}^{D}, \forall i \in \mathcal{B}^{DR}, t \tag{33}$$

$$\delta_{i,t}^{tra} \in \{0,1\}, \forall i \in \mathcal{B}^{DR}, t \tag{34}$$

The effective load at each bus consists of the served demand with DR adjustments and pump power consumption, as described in Eq. (35), while the reactive load is a constant power factor, as described in Eq. (36). The active and reactive power balances at each bus are finally enforced in Eqs. (37) and (38), respectively, with the power flow definitions in Eq. (39).

$$P_{i,t}^{load,eff} = \gamma_{i,t}^{P} \cdot P_{i,t}^{D} - P_{i,t}^{shift,dn} - P_{i,t}^{cur,dn} - P_{i,t}^{tra,dn} \\ + P_{i,t}^{shift,up} + P_{i,t}^{cur,up} + P_{i,t}^{tra,up} + \sum_{p \in \mathcal{P}_i^{pump}} P_{p,t}^{pump}, \forall i, t \tag{35}$$

$$Q_{i,t}^{load,eff} = \tan\phi_{load} \cdot P_{i,t}^{load,eff}, \forall i, t \tag{36}$$

$$P_{in} - P_{out} + \sum_{d:bus=i} P_{d,t}^{DG} + \sum_{p:bus=i} P_{p,t}^{PV} + \sum_{e:bus=i} P_{e,t}^{dis} \\ - \sum_{e:bus=i} P_{e,t}^{ch} = P_{i,t}^{load,eff}, \forall i, t \tag{37}$$

$$Q_{in} - Q_{out} \\ + \tan\phi_{DG} \left(\sum\nolimits_d P_{d,t}^{DG} + \sum\nolimits_p P_{p,t}^{PV} + \sum\nolimits_e P_{e,t}^{dis} \right) \\ = Q_{i,t}^{load,eff}, \forall i, t \tag{38}$$

$$P_{in} = \sum_{l:to(l)=i} P_{l,t}, P_{out} = \sum_{l:from(l)=i} P_{l,t} \\ , Q_{in} = \sum_{l:to(l)=i} Q_{l,t}, Q_{out} = \sum_{l:from(l)=i} Q_{l,t} \tag{39}$$

2.3. WDS Constraints

The WDS is characterized by a set of hydraulic constraints representing the steady state behavior of water flow and pressure through the network. The model includes mass conservation at each node, head loss in pipes, variable speed pump operation with discrete speed choice, and tank head volume dynamics. These constraints are formulated in a linearized MILP framework as in [10]. The mass balance at each water node must be satisfied, so that the total inflow is equal to the total outflow plus the demand served, as shown in Eq. (40). Inflow is water coming from connected pipes, pumps, the source and tank discharge. Outflow is water going to pipes, pumps, tank charging and the demand consumed. The continuous variable represents the fraction of water demand served at each node and is bounded between zero and one.

$$\sum_{l\in\mathcal{L}_n^{W,in}} Q_{l,t}^{W} + \sum_{p\in\mathcal{P}_n^{in}} Q_{p,t}^{pump} + Q_{n,t}^{source} + Q_{n,t}^{tank,out} = \sum_{l\in\mathcal{L}_n^{W,out}} Q_{l,t}^{W} + \sum_{p\in\mathcal{P}_n^{out}} Q_{p,t}^{pump} + Q_{n,t}^{tank,in} + W_{n,t}^{D}\cdot\gamma_{n,t}^{W}, \forall n,t \tag{40}$$

The head loss for each pipe is modeled using the nonlinear Hazen-Williams equation. In order to keep a linear MILP formulation, the equation is linearized by piecewise linear approximation technique as presented in [42]. The pipe flow is divided into K segments of equal length. The head loss is expressed as the sum of segment slopes times segment flows as in Eqs. (41)-(43). This is computationally feasible and correctly represents the nonlinear relation between flow and head-loss.

$$H_{n,t} - H_{m,t} = \sum_{k=1}^{K} \alpha_{l,k}\cdot Q_{l,k,t}^{seg}, \forall l=(n,m)\in\mathcal{L}^{W}, t \tag{41}$$

$$Q_{l,t}^{W} = \sum_{k=1}^{K} Q_{l,k,t}^{seg}, 0 \le Q_{l,k,t}^{seg} \le \frac{\bar{Q}_l^{W}}{K}, \forall l\in\mathcal{L}^{W}, t \tag{42}$$

$$\alpha_{l,k} = \frac{f_l\cdot\left[\left(\frac{k\cdot\bar{Q}_l^{W}}{K}\right)^{1.852} - \left(\frac{(k-1)\cdot\bar{Q}_l^{W}}{K}\right)^{1.852}\right]}{\frac{\bar{Q}_l^{W}}{K}}, \forall l\in\mathcal{L}^{W}, k=1,\dots,K \tag{43}$$

The modeling of variable-speed pumps is based on discrete speed levels to establish the relation between pump speed, flow rate, head rise and power consumption according to the MILP-based formulation proposed in [43]. A binary variable selects the operating speed level at each time step and another binary variable indicates the pump on/off status in Eq. (44). The pump flow is limited by the maximum flow capacity scaled by the selected speed, as enforced in Eq. (45). The head rise across the pump is expressed as a linear function of the selected speed and flow rate in Eq. (46) with the coefficients obtained from the pump characteristic curves. To make the problem a tractable MILP, the product of the binary speed selection and the continuous flow is linearized by introducing auxiliary variables in Eqs. (47)-(48). The power consumption of the pump is then calculated as linear function of the selected speed and flow rate in Eq. (49) and limited by the maximum pump power capacity in Eq. (50). Physically, this set of constraints allows the model to trade pumping intensity against available electricity: selecting a higher speed delivers more flow and head but draws proportionally more electrical power, so the pumps can be operated more aggressively only when the power network has spare capacity.

$$\sum_{r=1}^{R} \delta_{p,t,r}^{pump} = \chi_{p,t}^{pump}, \forall p\in\mathcal{P}^{pump}, t \tag{44}$$

$$0 \le Q_{p,t}^{pump} \le \bar{Q}_p^{pump}\cdot\sum_{r=1}^{R}\Omega_r\cdot\delta_{p,t,r}^{pump}, \forall p\in\mathcal{P}^{pump}, t \tag{45}$$

$$H_{m,t} - H_{n,t} = \sum_{r=1}^{R}\left(A_r\cdot\delta_{p,t,r}^{pump} - B_r\cdot Q_{p,t,r}^{lin}\right), \forall p=(n,m)\in\mathcal{P}^{pump}, t \tag{46}$$

$$Q_{p,t,r}^{lin} = \delta_{p,t,r}^{pump}\cdot Q_{p,t}^{pump}, \forall p\in\mathcal{P}^{pump}, r, t \tag{47}$$

$$0 \le Q_{p,t,r}^{lin} \le M\cdot\delta_{p,t,r}^{pump}, Q_{p,t,r}^{lin} \le Q_{p,t}^{pump}, Q_{p,t,r}^{lin} \ge Q_{p,t}^{pump} - M\cdot(1-\delta_{p,t,r}^{pump}), \forall p\in\mathcal{P}^{pump}, r, t \tag{48}$$

$$P_{p,t}^{pump} = \sum_{r=1}^{R}\left(C_r\cdot\delta_{p,t,r}^{pump} + D_r\cdot Q_{p,t,r}^{lin}\right), \forall p\in\mathcal{P}^{pump}, t \tag{49}$$

$$0 \le P_{p,t}^{pump} \le \bar{P}_p^{pump}\cdot\chi_{p,t}^{pump}, \forall p\in\mathcal{P}^{pump}, t \tag{50}$$

The dynamics of the water tanks are modeled according to the approach in [42] where the state variable is the volume of water stored in each tank in time. The volume at each time step is updated from the previous volume and the net inflow and outflow as given in Eq. (51). The tank volume is restricted by minimum and maximum capacities in Eq. (52) and the inflow and outflow rates are restricted in Eq. (53). The hydraulic head at the tank node is proportional to the stored volume with the proportionality factor being the tank surface area leading to the following head-volume relationship in Eq. (54). Finally, the hydraulic head at each node should be within the permissible limits to ensure the safe and reliable operation of the water distribution system as imposed in Eq. (55). Physically, Eq. (51) conserves the stored water, since the tank volume at each hour equals its previous volume plus the pumped inflow minus the released outflow. This is what gives the tank its buffering role: water can be stored when pumping capacity is available and released later when the electric supply constrains the pumps, thereby decoupling water delivery from the instantaneous state of the power network.

$$V_{k,t} = V_{k,t-1} + Q_{k,t}^{tank,in} - Q_{k,t}^{tank,out}, \forall k\in\mathcal{K}, t \tag{51}$$

$$V_k^{min} \le V_{k,t} \le V_k^{max}, \forall k\in\mathcal{K}, t \tag{52}$$

$$0 \le Q_{k,t}^{tank,in} \le \bar{Q}_k^{tank,in}, 0 \le Q_{k,t}^{tank,out} \le \bar{Q}_k^{tank,out}, \forall k\in\mathcal{K}, t \tag{53}$$

$$H_{k,t} = H_k^{base} + \frac{V_{k,t}}{A_k^{surface}}, \forall k\in\mathcal{K}, t \tag{54}$$

$$H_n^{min} \le H_{n,t} \le H_n^{max}, \forall n\in\mathcal{N}, t \tag{55}$$

2.4. Coupling Constraints

Coupling constraints explicitly couple the two infrastructures, capturing the interdependency between power and water distribution systems. The basic coupling between the networks stems from the fact that the power consumed by a water pump is proportional to the product of the pressure gain and flow rate as formulated in [44]. Eq. (56) expresses the total power consumed by water pumps at each bus by summation of power consumption of all pumps connected to that bus. The reactive power consumption of pumps is related to the constant power factor relationship in Eq. (57). This formulation correctly represents the electrical load of the water network in the PDS power balance equations.

$$P_{i,t}^{pump,total} = \sum_{p\in\mathcal{P}_i^{pump}} P_{p,t}^{pump}, \forall i\in\mathcal{B}, t \tag{56}$$

$$Q_{i,t}^{pump,total} = P_{i,t}^{pump,total}\cdot\tan\phi_i, \forall i\in\mathcal{B}, t \tag{57}$$

Finally, the demand served fractions of both electric and water demands are continuous variables between zero and one, which represent the restoration level of each load, as imposed in Eq. (58).

$$0 \le \gamma_{i,t}^{P} \le 1, 0 \le \gamma_{n,t}^{W} \le 1 \tag{58}$$

3. Case Studies and Results

The proposed framework is examined on a coupled test system consisting of a modified IEEE 33-bus PDS and a 15-node water distribution network. All simulations were carried out over a 24-hour restoration horizon in MATLAB using the YALMIP modeling layer [45], and the resulting MILP was solved with CPLEX to a relative optimality gap of 0.5%. All experiments were run on a desktop computer with an AMD Ryzen 5 processor and 24 GB of RAM. The remainder of this section describes the test system and input data, defines the studied cases, and then presents the restoration performance together with a detailed operational analysis.

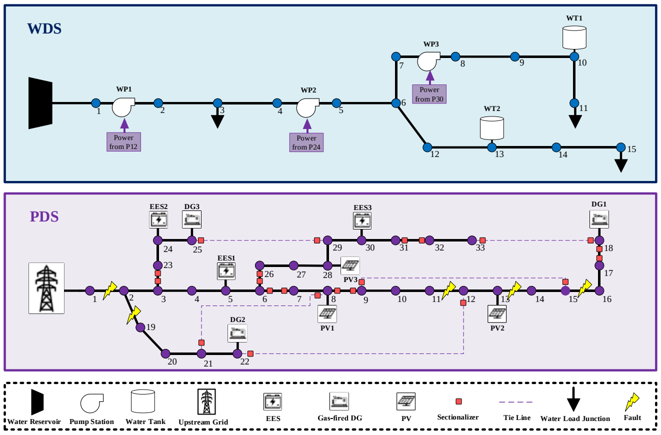

Fig. 2. Layout of coupled power and water distribution test system

3.1. Test System and Input Data

The layout of the coupled PDS and WDS, including the location of DERs, water facilities, damaged lines, and the electrical coupling between the two networks, is illustrated in Fig. 2. The PDS is based on the standard IEEE 33-bus radial network [46], operating in islanded mode, in which the connection to the upstream grid at bus 1 is severed following the disturbance. To emulate a severe HILP event, six distribution lines are assumed to be out of service, namely lines 1, 11, 13, 15, 18, and 23.

Restoration of the PDS is supported by a set of DERs. Three gas-fired distributed generators (DG1, DG2, and DG3) are placed at buses 18, 22, and 25, respectively, while three photovoltaic units (PV1, PV2, and PV3) are located at buses 8, 13, and 28. Three energy storage systems (EES1, EES2 and EES3) are installed at nodes 5, 24 and 30. In addition, five tie-lines and several sectionalizing switches allow the network to be reconfigured so that de-energized areas can be re-supplied through alternative routes after the faulty sections are isolated. The electric loads are classified according to their criticality and a priority weight is assigned to each class: the highest weight for critical loads (e.g. hospitals and emergency facilities), a lower weight for commercial loads, and a baseline weight for ordinary residential loads. This weighting steers the restoration toward the most vital loads when the available capacity is limited.

The 15-node WDS [32], comprises a single reservoir, three pump stations, two storage tanks, and three demand junctions. Water is delivered to consumers at nodes 3, 11, and 15, whereas storage is provided by tanks WT1 and WT2, connected near nodes 10 and 13. The three pumps WP1, WP2, and WP3 raise the hydraulic head across the network and, being energy-intensive, constitute the physical link to the power system. Their electrical demand is drawn from power buses 12, 24, and 30, so that any limitation in the available electric supply directly constrains the pumping capability and, consequently, the delivered water. Unlike the electric loads, all water demands are weighted equally, allowing the hydraulic constraints of the network, rather than an imposed prioritization, to determine how the limited supply is distributed among the consumers.

The key parameters of both systems are summarized in Table 2. The electrical and hydraulic demands follow representative 24-hour profiles with a pronounced midday peak, reflecting typical daily consumption patterns.

Table 2. System parameters and simulation settings

Category	Parameter	Value
General	Restoration horizon	24 h
	Power base	10 MVA
	Voltage limits	0.95-1.05 p.u.
	RI weighting factor (λ)	0.6
Distributed generators (DG1-DG3)	Connection buses	18, 22, 25
	Rated capacity (each)	0.75 MW
Photovoltaic units (PV1-PV3)	Connection buses	8, 13, 28
	Rated capacity (each)	0.20 MW
Energy storage (EES1–EES3)	Connection buses	5, 24, 30
	Energy capacity (each)	1 MWh
	Charge / discharge power	0.25 MW
	Charge / discharge efficiency	0.95 / 0.95
	Initial / minimum final SOC	50% / 10%
Electric load priority weights	Critical / commercial / residential	2.0 / 1.5 / 1.0
Demand response	Shiftable load share	20% of base load
	Curtailable load share	15% of base load
	Transferable load share	10% of base load
	Curtailment rebound (1-3 h)	60% / 30% / 10%
Water pumps (WP1-WP3)	Supplied from PDS buses	12, 24, 30
	Rated electrical power	350 / 250 / 150 kW
	Discrete speed levels	0.5, 0.7, 0.9, 1.0
Storage tanks	WT1 (node 10): max / initial	8000 / 2000 m³
	WT2 (node 13): max / initial	5400 / 1500 m³
	Minimum volume	100 m³
	Maximum in / out flow	800 m³/h
Disturbance	Out-of-service lines	1, 11, 13, 15, 18, 23
Solver settings	Hazen-Williams segments	3
	MILP optimality gap	0.5%

3.2. Description of Case Studies

To evaluate the contribution of the two flexibility mechanisms considered in this work, namely demand response and the hydraulic flexibility offered by water storage, and at the same time to demonstrate the value of coordinating the two networks, the restoration problem is solved under five cases. In all cases, network reconfiguration and the dispatch of distributed energy resources remain active, so that the cases differ only in the flexibility mechanisms enabled and in whether the two systems are restored jointly or independently.

Case 1 is a decoupled benchmark that reflects the conventional practice of restoring the two infrastructures separately. Here, the power network is restored with absolute priority, and the pumps of the water network receive only the electric capacity that remains after the ordinary electric loads have been served, without any coordination between the two operators. This case enables both flexibility mechanisms but lacks the joint optimization of the proposed framework, and it therefore serves as a reference against which the benefit of coordination is measured.

The remaining four cases apply the proposed coordinated formulation and are ordered by increasing resilience. Case 2 is the coordinated baseline, in which both DR and tank flexibility are disabled: the storage tanks are held at their initial volume and cannot exchange water with the network, and no load is shifted, curtailed, or transferred. Case 3 activates the demand response programs while keeping the tanks inactive, exposing the isolated effect of demand-side flexibility. Case 4 enables the hydraulic flexibility of the tanks while demand response remains disabled, revealing the contribution of water storage alone. Finally, Case 5 combines both mechanisms and represents the fully coordinated restoration strategy proposed in this paper. A summary of the five cases is provided in Table 3.

3.3. Restoration Performance and Comparative Analysis

The overall restoration performance of the five cases is summarized in Table 4 and Fig. 3, which report the electric restoration index, the water restoration index, the composite resilience index, and the total unserved electric and water demand over the horizon. The four coordinated cases (Cases 2 to 5) are examined first, followed by a separate discussion of the decoupled benchmark in Case 1.

Table 3. Definition of the five case studies and the flexibility mechanisms enabled in each

Case	Coordination	Reconfiguration & DER dispatch	Demand response	Hydraulic (tank) flexibility
Case 1	✗	✓	✓	✓
Case 2	✓	✓	✗	✗
Case 3	✓	✓	✓	✗
Case 4	✓	✓	✗	✓
Case 5	✓	✓	✓	✓

Table 4. Restoration performance indices for the five cases

Metric	Case 1	Case 2	Case 3	Case 4	Case 5
R_{PDS}	0.8859	0.7956	0.8135	0.7919	0.8086
R_{WDS}	0.2698	0.2702	0.2681	0.6381	0.6382
RI (composite)	0.6394	0.5854	0.5953	0.7304	0.7404
Electric shedding (p.u.)	1.067	1.9119	1.7163	1.9462	1.7569
Water curtailment (m^3)	6892.0828	6887.5273	6908.1274	3415.8991	3414.6679

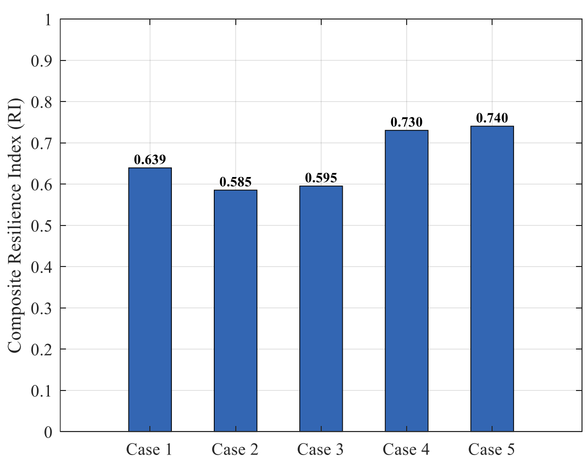

Fig. 3. Composite resilience index for the five cases

Among the four coordinated cases, the composite resilience index increases steadily, from 0.5854 in the baseline to 0.7404 in the fully coordinated strategy, confirming that the progressive activation of the flexibility mechanisms consistently strengthens the recovery of the coupled system. This ranking is visualized in Fig. 3, where the index is seen to rise markedly once hydraulic flexibility is introduced.

A closer inspection reveals that the two mechanisms act on different parts of the coupled system. DR, activated in Case 3, primarily benefits the power network: relative to the coordinated baseline in Case 2, the electric restoration index improves from 0.7956 to 0.8135, and the total electric load shedding decreases from 1.91 p.u. to 1.72 p.u. Its effect on the water side is negligible, as the water restoration index remains essentially unchanged at about 0.27. This behavior is expected, since DR redistributes electrical consumption over time while conserving the total daily energy; it relieves the power network during peak hours but does not, on its own, create additional pumping capability for the water system.

The hydraulic flexibility of the storage tanks, enabled in Case 4, exhibits the opposite and considerably stronger behavior. The water restoration index rises from about 0.27 to 0.64, more than doubling, while the total water curtailment is nearly halved, decreasing from about 6888 m^3 to 3416 m^3. This pronounced gain arises because the tanks allow water to be pumped and stored during hours when the electric supply is comparatively abundant and released later during peak-demand hours, when pumping would otherwise be constrained. In effect, the tanks partially decouple water delivery from the instantaneous limitations of the power network. It is worth noting, however, that activating hydraulic flexibility slightly lowers the electric restoration index in Case 4 relative to Case 2, from 0.7956 to 0.7919. This apparent trade-off is a direct manifestation of the interdependency between the two networks: when the tanks are allowed to store water, the pumps operate more intensively and impose an additional electrical load on the power system, which competes with the ordinary electric loads for the limited generation capacity. The effect is modest and is far outweighed by the substantial improvement in water restoration, but it illustrates that hydraulic flexibility is not entirely free from the power side and that the coupling between the two infrastructures operates in both directions.

When both mechanisms are combined in Case 5, the coordinated strategy attains the highest resilience among all cases, with RI reaching 0.7404. Relative to Case 4, the additional demand-side flexibility improves the electric restoration index from 0.7919 to 0.8086, since DR partially offsets the extra pumping load introduced by the tanks by reshaping the electric demand away from the critical hours, while the water restoration index remains essentially unchanged. The two mechanisms therefore operate in a complementary fashion: the tanks carry the bulk of the water-side restoration, while DR tightens the power-side recovery and mitigates the additional burden that intensive pumping places on the network. The largest share of the resilience gain thus originates from hydraulic flexibility, whereas DR contributes a smaller but consistent improvement.

Finally, the decoupled benchmark in Case 1 reveals the value of coordination itself. Because the power network is restored with absolute priority, Case 1 attains the highest electric restoration index of 0.8859, even exceeding that of the fully coordinated strategy. This advantage, however, comes at the expense of the water side. Although Case 1 has access to the storage tanks, the pumps receive almost no electric capacity once the ordinary electric loads have been served, so the tanks cannot be meaningfully refilled and remain largely unused. As a result, the water restoration index of Case 1 falls to 0.2698, essentially the same level as the coordinated baseline in Case 2, which reaches 0.2702 with the tanks disabled altogether. In other words, without coordination the hydraulic flexibility of the network is effectively wasted, since the tanks are of no use unless the power system is operated so as to leave capacity for pumping. Consequently, the composite resilience index of Case 1 falls to 0.6394, well below the 0.7404 of the fully coordinated strategy, which shows that jointly optimizing the two networks yields a more resilient overall system than restoring them independently.

For each case, the resulting MILP contains 2191 binary variables together with the associated continuous variables and constraints. The solution times of the five cases are reported in Table 5.

Table 5. Solution time of the MILP model for the five cases

Case	Case 1	Case 2	Case 3	Case 4	Case 5
Solve time (s)	303.6	92.0	612.0	168.7	609.4

The solution times reveal that the computational burden is governed primarily by the DR programs rather than by the hydraulic flexibility. The coordinated baseline in Case 2, which activates neither mechanism, is solved in 92 s, whereas enabling the tanks alone in Case 4 increases the time only moderately to 168.7 s. In contrast, the two cases that activate DR, namely Case 3 and Case 5, require 612.0 s and 609.4 s respectively, roughly four times longer than Case 4. This behavior follows from the structure of the DR formulation: the curtailable and transferable programs introduce binary switching variables at every bus and time step, together with rebound and transfer-window constraints that couple decisions across several consecutive hours. The resulting combinatorial structure is considerably harder for the branch-and-bound search than the tank dynamics, which involve continuous volume variables linked by simple balance equations. The decoupled benchmark in Case 1 lies in between, at 303.6 s, since its hierarchical objective narrows the search on the water side once the electric restoration has been prioritized. In all cases, however, the model is solved within roughly ten minutes, which confirms the tractability of the fully linearized formulation for a system of this size.

3.4. Operational Analysis

Further insight into the restoration process is obtained by examining the temporal behavior of the two subsystems. Fig. 4 presents the restored electric and water loads over the 24-hour horizon. On the electric side, all five cases track the demand profile closely throughout the horizon, in agreement with the high electric restoration indices; the small differences among the cases reflect the limited room for improvement once the distributed generators, storage units, and network reconfiguration are dispatched. On the water side, the contrast is stark: in Cases 2 and 3 the delivered water falls sharply after the early hours and remains well below demand, whereas in Cases 4 and 5 a substantially higher level of delivery is sustained throughout the peak period. Case 1 follows the same depressed pattern as Cases 2 and 3, since the pumps are left with too little electric capacity for the tanks to be of practical use.

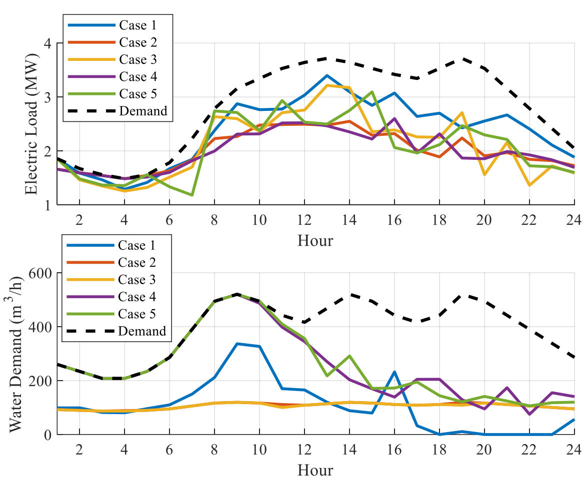

Fig. 4. Restored electric and water loads over the 24-hour horizon

The mechanism underlying this behavior is clarified by Fig. 5, which shows the stored volume in the two tanks over the horizon. In Cases 2 and 3, where hydraulic flexibility is disabled, the tank volumes remain fixed at their initial values, since the tanks are prevented from exchanging water with the network. Once flexibility is enabled in Cases 4 and 5, both tanks progressively discharge during the day to supplement pumping, and the stored volume is drawn down as the tanks release water to meet demand during the hours in which the electric supply limits the pumps. In Case 1 the tanks are nominally available, yet their stored volume changes only marginally, since the pumps receive almost no electric capacity and the tanks can therefore be neither refilled nor usefully drawn upon.

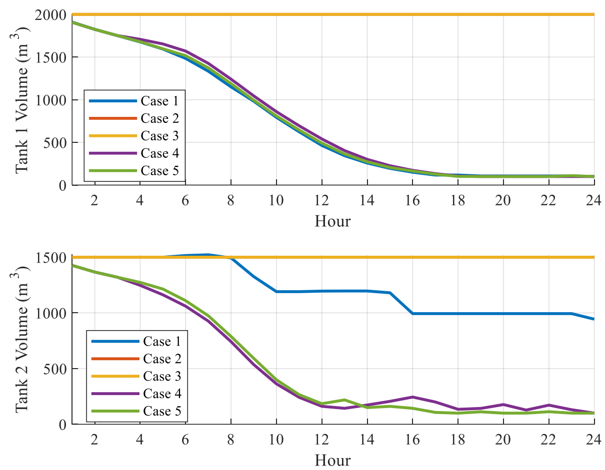

Fig. 5. Stored volume in the two tanks over the horizon

The operational decisions behind these results are summarized in Table 6, which reports the status of the switchable lines in each case. Lines 1, 13, and 18 remain open in all cases, since they coincide with the faulted sections that must be isolated, while the remaining tie-lines and sectionalizers are closed to re-energize the disconnected regions through alternative paths. The resulting topology is almost identical across the five cases, which indicates that the reconfiguration is dictated primarily by the location of the faults rather than by the flexibility mechanisms. The only exception is line 37, which is opened in Cases 3 and 5: with DR active, part of the peak load is shifted away in time, so this path is no longer required and the optimizer selects a slightly different radial configuration.

Table 6. Switch status per case

Line	Case 1	Case 2	Case 3	Case 4	Case 5
L1	0	0	0	0	0
L6	1	1	1	1	1
L8	1	1	1	1	1
L13	0	0	0	0	0
L18	0	0	0	0	0
L22	1	1	1	1	1
L25	1	1	1	1	1
L31	1	1	1	1	1
L33	1	1	1	1	1
L34	1	1	1	1	1
L35	1	1	1	1	1
L36	1	1	1	1	1
L37	1	1	0	1	0

The hourly electric load shedding is reported in Table 7 and illustrated in Fig. 6. In all five cases the shedding remains small throughout the horizon, consistent with the high electric restoration indices and reflecting the ability of the distributed generation, storage, and reconfiguration to re-supply most of the load in islanded operation. The shed quantities follow the daily demand profile, staying near zero in the early hours and rising toward the midday and evening peaks, when the load approaches the available capacity. The shedding is consistently reduced whenever demand response is active, so that Cases 3 and 5 outperform Cases 2 and 4 during the peak hours. This confirms that the main contribution of demand response is on the power side, where it relieves the network during the most heavily loaded hours by reshaping the flexible load toward periods of higher supply availability.

Table 7. Hourly electric load shedding (p.u.) for the five cases

Hour	Case 1	Case 2	Case 3	Case 4	Case 5
1	0.0000	0.0195	0.0000	0.0198	0.0000
2	0.0083	0.0077	0.0208	0.0080	0.0189
3	0.0096	0.0014	0.0210	0.0018	0.0193
4	0.0197	0.0000	0.0231	0.0001	0.0128
5	0.0144	0.0016	0.0237	0.0044	0.0000
6	0.0112	0.0150	0.0269	0.0181	0.0448
7	0.0385	0.0397	0.0530	0.0410	0.1049
8	0.0405	0.0557	0.0152	0.0788	0.0046
9	0.0283	0.0891	0.0560	0.0846	0.0446
10	0.0579	0.0865	0.0983	0.1027	0.0966
11	0.0753	0.1040	0.0820	0.1011	0.0595
12	0.0606	0.1146	0.0883	0.1118	0.1107
13	0.0317	0.1238	0.0501	0.1251	0.1217
14	0.0546	0.1092	0.0467	0.1289	0.0889
15	0.0685	0.1238	0.1174	0.1308	0.0435
16	0.0345	0.1097	0.1028	0.0819	0.1355
17	0.0705	0.1328	0.1083	0.1382	0.1380
18	0.0830	0.1640	0.1277	0.1213	0.1413
19	0.1287	0.1475	0.1006	0.1847	0.1246
20	0.0975	0.1621	0.1970	0.1674	0.1232
21	0.0491	0.1188	0.1000	0.1169	0.0946
22	0.0379	0.0943	0.1423	0.0860	0.1062
23	0.0306	0.0595	0.0693	0.0580	0.0710
24	0.0160	0.0317	0.0455	0.0349	0.0443
Total	1.0670	1.9119	1.7161	1.9462	1.7494

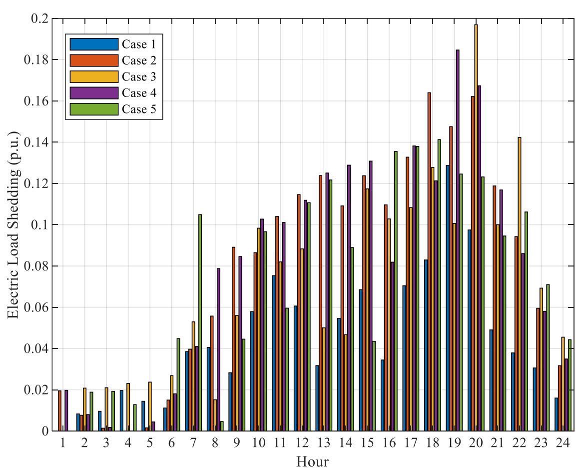

Fig. 6. Hourly electric load shedding for the five cases

The hourly water curtailment is reported in Table 8 and illustrated in Fig. 7, where the decisive role of hydraulic flexibility is immediately apparent. In Cases 2 and 3, with the tanks inactive, the curtailment is high and virtually identical throughout the horizon, since without storage the delivered water is bound directly to the limited pumping capability; the near-perfect overlap between the two cases further confirms that demand response alone brings no benefit to the water side. In Cases 4 and 5, by contrast, the curtailment drops sharply. It falls to zero during the early hours, as the tanks fully cover the demand from their initial volume, and reappears only later as the stored volume is gradually depleted, yet remains well below the levels of Cases 2 and 3. The tanks thus act as a temporal buffer that decouples water delivery from the momentary limitations of the power network, which is the principal mechanism behind the improvement in the water restoration index.

Table 8. Hourly water curtailment (m^3/h) for the five cases

Hour	Case 1	Case 2	Case 3	Case 4	Case 5
1	161.26	167.69	167.69	0.00	0.00
2	135.06	144.38	144.39	0.00	0.00
3	126.24	121.06	121.10	0.00	0.00
4	127.23	119.35	121.10	0.00	0.00
5	138.04	144.33	144.39	0.00	0.00
6	176.00	190.98	190.98	0.00	0.00
7	240.00	284.15	284.09	0.00	0.00
8	282.18	377.32	377.31	0.00	0.00
9	183.51	400.61	400.61	0.00	0.00
10	167.48	377.32	377.32	7.56	0.00
11	272.00	330.73	341.97	43.78	32.32
12	250.88	307.44	307.44	71.43	60.07
13	348.28	354.02	354.02	198.11	250.54
14	431.66	400.61	400.61	316.90	228.86
15	414.40	377.32	377.32	324.52	322.95
16	209.86	330.73	330.73	303.19	269.70
17	383.39	307.44	307.44	211.40	221.24
18	442.00	330.73	330.73	237.23	297.98
19	509.11	400.61	411.25	390.72	398.86
20	494.00	377.32	377.32	399.00	352.76
21	442.00	330.73	330.73	268.53	317.80
22	390.00	284.15	284.15	315.00	283.83
23	338.00	237.56	237.56	183.06	219.99
24	229.50	190.98	190.98	145.47	166.07
Total	6892.08	6887.53	6911.22	3415.90	3422.96

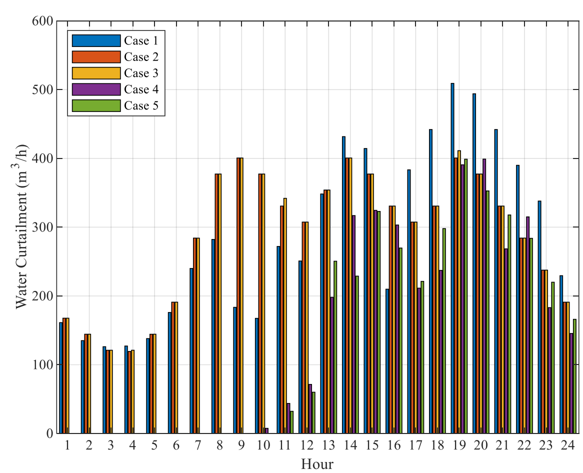

Fig. 7. Hourly water curtailment for the five cases

The effect of DR on the load profile is examined in Figs. 8 and 9, which show the electric demand before and after the application of the demand-response programs in Cases 3 and 5, respectively. The programs shift and curtail a portion of the flexible load away from the critical peak hours and redistribute it toward periods of higher supply availability, while preserving the total daily energy consumption.

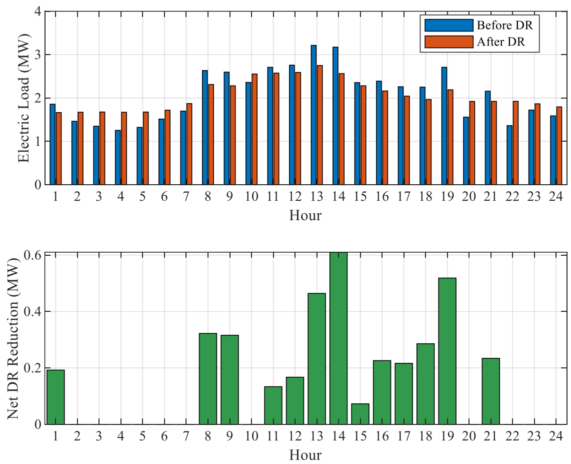

Fig. 8. Electric demand before and after DR in Case 3

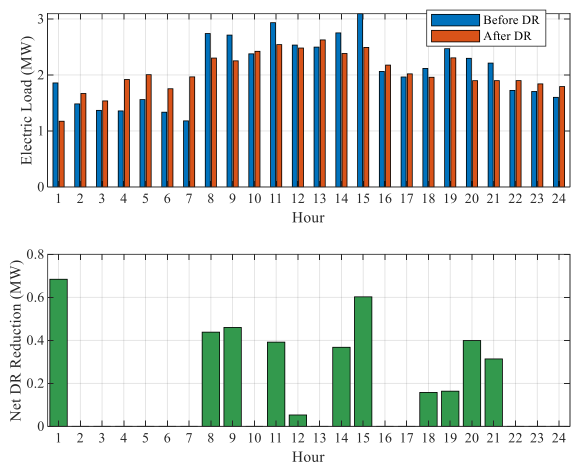

Fig. 9. Electric demand before and after DR in Case 5

The bus voltage magnitudes across the network are presented as heatmaps in Figs. 10–14 for Cases 1 to 5, respectively. In each heatmap, the horizontal axis denotes the 24-hour horizon and the vertical axis the bus index, while the color scale represents the voltage magnitude. Across all five cases, the energized buses remain within the permissible band of 0.95–1.05 p.u. throughout the entire restoration horizon, with the majority of buses maintained close to the nominal value. A mild reduction in voltage is observed during the midday and evening peak-demand hours, when the loading of the network is highest and the distributed resources operate closer to their limits; this pattern is consistent with the increased load shedding reported for those hours in Table 7. The main substation bus, which is disconnected during islanded operation, is excluded from the energized region and therefore appears distinctly in the maps. Importantly, the introduction of DR and hydraulic flexibility does not induce any voltage violations; on the contrary, by relieving the network during the most heavily loaded hours, these mechanisms help maintain a stable voltage profile across the restoration horizon. This confirms that the proposed coordinated restoration strategy improves the recovery of both critical loads without compromising the operational security of the PDS.

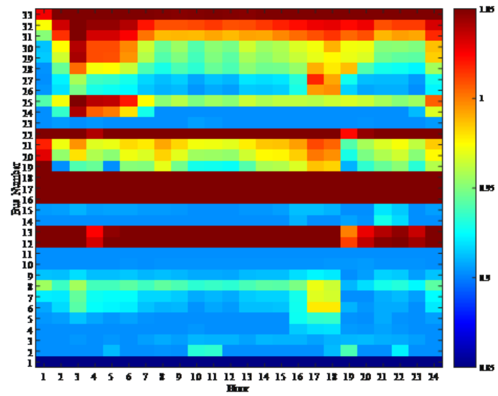

Fig. 10. Bus voltage heatmap for Case 1

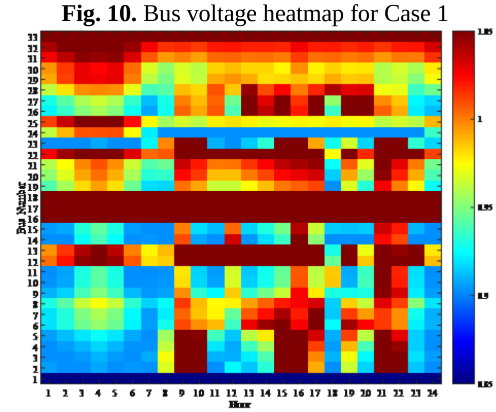

Fig. 11. Bus voltage heatmap for Case 2

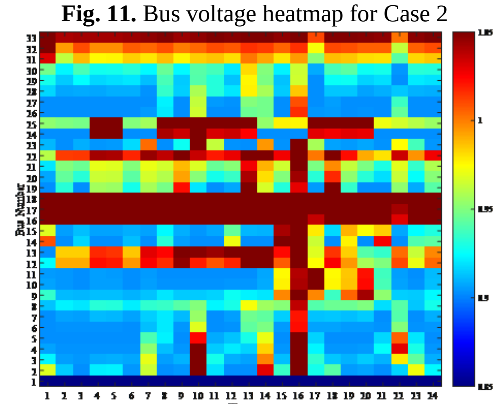

Fig. 12. Bus voltage heatmap for Case 3

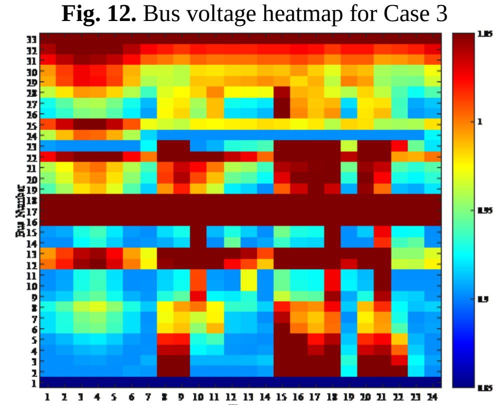

Fig. 13. Bus voltage heatmap for Case 4

To justify the choice of the weighting factor and to examine its influence on the restoration outcome, a sensitivity analysis was carried out by re-solving the fully coordinated case for values of λ ranging from 0.05 to 1.00 in steps of 0.05, with the results reported in Fig. 15. As expected, increasing λ shifts the restoration effort toward the power side: the electric restoration index rises steadily from 0.7897 at the lowest weight to 0.8864 when the objective is placed entirely on the electric loads, while the water restoration index declines from 0.6508 to 0.2415 over the same range. The transition, however, is far from uniform. For weights up to about 0.65 the water restoration index remains within a narrow band around 0.64, so that a growing priority on the electric loads is accommodated with almost no penalty on the water side. Beyond this point the behavior changes sharply, and the water index collapses to 0.6196 at a weight of 0.65, to 0.4034 at 0.85, and finally to 0.2415 when water is excluded from the objective altogether. The value of 0.6 adopted in this study therefore lies at the upper end of the stable region: it assigns a slightly higher priority to electric service, consistent with the criticality of power supply during emergencies, while the water restoration index remains within about two and a half percent of its maximum attainable value. It should be noted that the composite index itself is not directly comparable across different weights, since its definition changes with λ; the meaningful comparison is between the two component indices, which is what Fig. 15 displays.

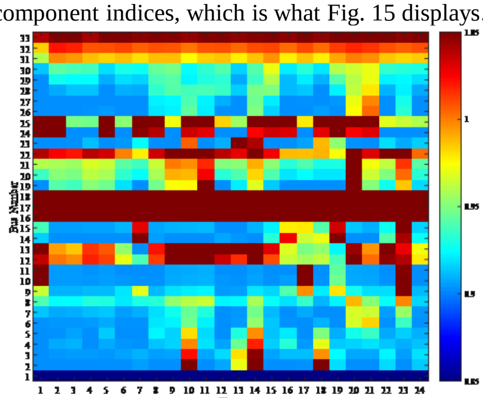

Fig. 14. Bus voltage heatmap for Case 5

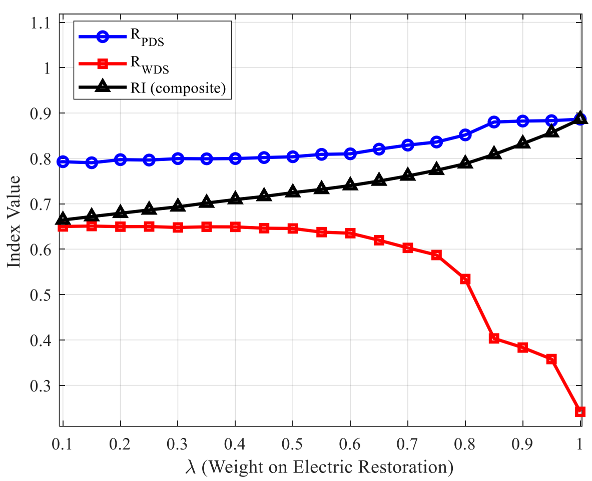

Fig. 15. Sensitivity of restoration indices to weighting factor (λ)

Overall, the results confirm that the coordinated restoration of the coupled PDS and WDS benefits from both flexibility mechanisms, although to a remarkably different extent. Hydraulic flexibility emerges as the dominant contributor, raising the water restoration index from about 0.27 to 0.64 and driving most of the improvement in the composite resilience index, whereas DR plays a complementary role by relieving the power network during peak hours and partially offsetting the additional pumping load introduced by the tanks. Their combined use in the fully coordinated strategy yields the highest overall resilience, demonstrating that jointly exploiting demand-side and hydraulic flexibility provides the most effective restoration of the two interdependent infrastructures.

4. Conclusions

In this study, a fully linearized MILP framework was developed for the resilience-oriented restoration of coupled power and water distribution systems following a HILP disturbance. The framework embeds the operational constraints of both infrastructures, including network reconfiguration, DER dispatch, hydraulic head losses, variable-speed pump operation, and tank storage dynamics, within a single optimization model, and coordinates them through nexus constraints together with three DR programs. To evaluate the individual and combined contributions of the flexibility mechanisms, and to quantify the value of coordination itself, five cases were solved on a coupled IEEE 33-bus power system and a 15-node water network, including a decoupled benchmark in which the two networks are restored independently. The results demonstrate that hydraulic flexibility is the dominant contributor to resilience, raising the water restoration index from about 0.27 to 0.64, whereas DR plays a complementary role by relieving the power network during peak hours and offsetting the additional pumping load introduced by the tanks. Their coordinated use yields the highest overall resilience, and the comparison with the decoupled benchmark shows that restoring the two networks independently wastes the available hydraulic flexibility, since the tanks cannot be refilled once the power system is operated without regard for pumping. These findings can help system operators prioritize restoration resources and highlight the value of treating water storage as an active flexibility asset during emergencies. The present study is nevertheless subject to certain limitations, which also define the directions for future work. It adopts a deterministic setting in which the fault pattern, the load profiles, and the photovoltaic generation are assumed known; extending the framework to account for the uncertainty of HILP events, renewable generation, and demand, through scenario-based, robust, or stochastic formulations, would allow the restoration strategy to be assessed under a realistic range of operating conditions and would naturally lead to a resilience-oriented planning problem in which the siting and sizing of distributed resources and storage are optimized alongside their operation. In addition, the disturbance considered here affects only the power network, whereas real events may simultaneously damage pumps, tanks, and water pipes, so incorporating combined failure scenarios on both infrastructures is a valuable extension.

References

[1] T. Sun, C. Zanocco, J. Flora, A. Sheshadri, and R. Rajagopal, "Unified 0.25-degree gridded infrastructure-critical extreme weather for the United States from 1979 to 2100", *Sci. Data*, vol. 12, p. 1544, 2025.

[2] G. Pescaroli, L. McMillan, M. Gordon, N. Y. Aydin, T. Comes, M. Maraschini, J. Oliveira Palmas, S. Torresan, B. Trump, M. Pelling, and I. Linkov, "Definitions and taxonomy for High Impact Low Probability (HILP) and outlier events", *Int. J. Disaster Risk Reduct.*, vol. 127, p. 105504, 2025.

[3] A. Nasri, A. Abdollahi, and M. Rashidinejad, "Multi-stage and resilience-based distribution network expansion planning against hurricanes based on vulnerability and resiliency metrics", *Int. J. Electr. Power Energy Syst.*, vol. 136, p. 107640, 2022.

[4] T. Aruväli, M. De Marchi, and E. Rauch, "Analysis of quantitative metrics for assessing resilience of human-centered CPPS workstations", *Sci. Rep.*, vol. 13, p. 2914, 2023.

[5] D. A. Bromberger, V. J. Garcia, S. D. Rodrigues, and L. S. Neves, "A taxonomy for extreme weather events and their impacts on power systems: A comprehensive review of classification, effects, and mitigation strategies", *Renew. Sustain. Energy Rev.*, vol. 227, p. 116498, 2026.

[6] K. V. S. M. Babu, D. Dwivedi, P. Chakraborty, P. K. Yemula, and M. Pal, "A comprehensive review on resilience definitions, frameworks, metrics, and enhancement strategies in electrical

distribution systems", *Appl. Energy*, vol. 394, p. 126141, 2025.

[7] S. Qaeini, A. Abdollahi, and M. Rashidinejad, "A tri-stage stochastic resilience-oriented expansion planning of a smart distribution network under cyber-physical attacks considering IRP mitigation strategy", *Sustain. Energy, Grids Networks*, vol. 42, p. 101701, 2025.

[8] M. A. Gilani, R. Dashti, M. Ghasemi, M. H. Amirioun, and M. Shafie-khah, "A microgrid formation-based restoration model for resilient distribution systems using distributed energy resources and demand response programs", *Sustain. Cities Soc.*, vol. 83, p. 103975, 2022.

[9] M. Izadi, S. H. Hosseinian, S. Dehghan, A. Fakharian, and N. Amjady, "Resiliency-Oriented operation of distribution networks under unexpected wildfires using Multi-Horizon Information-Gap decision theory", *Appl. Energy*, vol. 334, p. 120536, 2023.

[10] L. Rodriguez-Garcia, M. Panteli, and M. Parvania, "Coordinated recovery of interdependent power and water distribution systems", *IET Smart Grid*, vol. 7, pp. 760-775, 2024.

[11] S. Mohammaddini, H. Yousefi, M. Abdoos, M. Allahrabbi Shirazi, and A. Hajinezhad, "Techno-economic simulation of solar flat plate collector systems for building hot water demand supply", *Energy*, vol. 338, p. 138933, 2025.

[12] M. Allahrabbi Shirazi, H. Yousefi, A. Fathi, and M. Baneshi, "Urban Water Sustainability through Energy-Free Fog Water Harvesting: A Review of Fog-Collecting Systems", *Urban Dev. Policy Mak.*, vol. 3, pp. 69-94, 2026.

[13] A. Saifoddin, M. H. Gholizadeh, and M. Allahrabbi Shirazi, "Integrated analysis of advanced applications of artificial intelligence (AI) in modern energy systems", *J. Sustain. Energy Syst.*, vol. 5, pp. 297-327, 2026.

[14] A. Arjomandi-Nezhad, M. Fotuhi-Firuzabad, M. Moeini-Aghtaie, A. Safdarian, P. Dehghanian, and F. Wang, "Modeling and Optimizing Recovery Strategies for Power Distribution System Resilience", *IEEE Syst. J.*, vol. 15, pp. 4725-4734, 2021.

[15] S. Poudel and A. Dubey, "Critical Load Restoration Using Distributed Energy Resources for Resilient Power Distribution System", *IEEE Trans. Power Syst.*, vol. 34, pp. 52-63, 2019.

[16] Q. Shi, F. Li, J. Dong, M. Olama, X. Wang, C. Winstead, and T. Kuruganti, "Co-optimization of repairs and dynamic network reconfiguration for improved distribution system resilience", *Appl. Energy*, vol. 318, p. 119245, 2022.

[17] S. Najafi Ravadanegh, M.-R. Jannati-Oskuee, and G. B. Gharehpetian, "Resiliency-oriented dynamic expansion planning of MG-based distribution networks", *J. Energy Manag. Technol.*, vol. 6, pp. 44-53, 2022.

[18] M. Foroughifard, A. Abdollahi, M. Rashidinejad, S. Mobasheri, and A. Riki, "Resilience-Oriented Planning of Active Distribution Networks via A Bilevel System of Systems Approach", *Smart Grid Conf. SGC*, pp. 1-6, 2025.

[19] M. Ghasemi, A. Kazemi, E. Bompard, and F. Aminifar, "A two-stage resilience improvement planning for power distribution systems against hurricanes", *Int. J. Electr. Power Energy Syst.*, vol. 132, p. 107214, 2021.

[20] S. Behzadi and A. Bagheri, "A trade-off between line hardening and dynamic line rating by a new convex optimization model for resilient micro-grid-oriented expansion planning of reconfigurable smart distribution networks incorporated with renewable energy sources", *Next Energy*, vol. 8, p. 100351, 2025.

[21] R. Saberi, H. Falaghi, M. Esmaeeli, and M. Ramezani, "A two-stage approach to enhance distribution network resilience against natural disasters", *J. Energy Manag. Technol.*, vol. 5, pp. 53-63, 2021.

[22] H. Wan, W. Liu, S. Zhang, Q. Shi, R. Cheng, and W. Feng, "Resilience-oriented load restoration method for power-gas-water systems considering public safety impact", *IET Gener. Transm. Distrib.*, vol. 18, pp. 3350-3364, 2024.

[23] Y. Zhang, H. Zhang, S. Wang, Z. Li, R. R. Tan, F. Wang, and X. Jia, "Vulnerability analysis of water systems to power interruptions in critical infrastructures", *Sustain. Energy, Grids Networks*, vol. 46, p. 102248, 2026.

[24] J. Li, Y. Xu, Y. Wang, M. Li, J. He, C.-C. Liu, and K. P. Schneider, "Resilience-Motivated Distribution System Restoration Considering Electricity-Water-Gas Interdependency", *IEEE Trans. Smart Grid*, vol. 12, pp. 4799-4812, 2021.

[25] A. Tiong and H. A. Vergara, "A two-stage stochastic multi-objective resilience optimization model for network expansion of interdependent power-water networks under disruption", *Int. J. Crit. Infrastruct. Prot.*, vol. 40, p. 100588, 2023.

[26] A. Stuhlmacher and J. L. Mathieu, "Flexible drinking water pumping to provide multiple grid services", *Electr. Power Syst. Res.*, vol. 212, p. 108491, 2022.

[27] J. Najafi, A. Peiravi, and A. Anvari-Moghaddam, "Enhancing Integrated Power and Water Distribution Networks Seismic Resilience Leveraging Microgrids", *Sustainability*, vol. 12, p. 2167, 2020.

[28] H. Cui, W. Xia, S. Yang, and X. Wang, "Real-time emergency demand response strategy for optimal load dispatch of heat and power micro-grids", *Int. J. Electr. Power Energy Syst.*, vol. 121, p. 106127, 2020.

[29] V. Sharifi, A. Abdollahi, M. Rashidinejad, E. Heydarian-Forushani, and H. H. Alhelou, "Integrated Electricity and Natural Gas Demand Response in Flexibility-Based Generation Maintenance Scheduling", *IEEE Access*, vol. 10, pp. 76021-76030, 2022.

[30] C. Essayeh, M. Raiss El-Fenni, H. Dahmouni, and M. A. Ahajjam, "Energy Management Strategies for Smart Green MicroGrid Systems: A Systematic Literature Review", *J. Electr. Comput. Eng.*, vol. 2021, p. 6675975, 2021.

[31] S. Poorvaezi Roukerd, A. Abdollahi, and M. Rashidinejad, "Uncertainty-based unit commitment and construction in the presence of fast ramp units and energy storages as flexible resources considering enigmatic demand elasticity", *J. Energy Storage*, vol. 29, p. 101290, 2020.

[32] K. Oikonomou and M. Parvania, "Optimal Coordination of Water Distribution Energy Flexibility With Power Systems Operation", *IEEE Trans. Smart Grid*, vol. 10, pp. 1101-1110, 2019.

[33] R. Ghaffarpour, B. Mozafari, A. M. Ranjbar, and T. Torabi, "Resilience oriented water and energy hub scheduling considering maintenance constraint", *Energy*, vol. 158, pp. 1092-1104, 2018.

[34] P. Juan-García, L. Rieger, G. Darch, O. Schraa, and L. Corominas, "A framework for model-based assessment of resilience in water resource recovery facilities against power outage", *Water Res.*, vol. 202, p. 117459, 2021.

[35] M. Arabsadegh and A. Doroudi, "Resilience-Oriented Restoration After Storm-Induced Failures Using Genetic Algorithm and Probabilistic Circuit Breaker Modeling", *Iran. J. Electr. Electron. Eng.*, vol. 21, pp. 151-168, 2025.

[36] M. Karimi and M. Eslamian, "A Resilience-Oriented Graph-Based Method for Restoration of Critical Loads in Distribution Networks Using Microgrids", *J. Oper. Autom. Power Eng.*, vol. 13, pp. 99-109, 2025.

[37] J. Khayatzadeh, S. M. Ezzati, and A. Monjazebi, "Economical operation of energy hub by using energy storage systems focusing on resilience and energy security indices", *J. Energy Manag. Technol.*, vol. 8, pp. 295-306, 2024.

[38] H. Wan, W. Liu, Q. Shi, R. Zhu, X. Zhang, and J. Zhao, "Real-Time Service Restoration of Coupled Power-Water Systems Considering the Spatio-Temporal Cascading Failure", *IEEE Trans. Smart Grid*, vol. 17, pp. 178-192, 2026.

[39] B. A. Alkhaleel, H. Liao, and K. M. Sullivan, "Model and solution method for mean-risk cost-based post-disruption restoration of

interdependent critical infrastructure networks”, *Comput. Oper. Res.*, vol. 144, p. 105812, 2022.

[40] W. Shi, H. Liang, and M. Bittner, “Dynamic microgrid formation for resilient distribution systems considering large-scale deployment of mobile energy resources”, *Appl. Energy*, vol. 362, p. 122978, 2024.

[41] S. Dorahaki, M. Rashidinejad, S. F. Fatemi Ardestani, A. Abdollahi, and M. R. Salehizadeh, “A Peer-to-Peer energy trading market model based on time-driven prospect theory in a smart and sustainable energy community”, *Sustain. Energy, Grids Networks*, vol. 28, p. 100542, 2021.

[42] C. Hallmann and L. Suhl, “Optimizing water tanks in water distribution systems by combining network reduction, mathematical optimization and hydraulic simulation”, *OR Spectr.*, vol. 38, pp. 577-595, 2016.

[43] T. Janus, B. Ulanicki, and K. Diao, “Optimal scheduling of variable speed pumps with mixed integer linear programming”, *Water Supply*, vol. 24, pp. 2409-2426, 2024.

[44] A. S. Zamzam, E. Dall’Anese, C. Zhao, J. A. Taylor, and N. D. Sidiropoulos, “Optimal Water-Power Flow-Problem: Formulation and Distributed Optimal Solution”, *IEEE Trans. Control Netw. Syst.*, vol. 6, pp. 37-47, 2019.

[45] J. Löfberg, “YALMIP: A toolbox for modeling and optimization in MATLAB”, *Proc. 2004 IEEE Int. Symp. Computer Aided Control Systems Design*, pp. 284-289, 2004.

[46] S. H. Dolatabadi, M. Ghorbanian, P. Siano, and N. D. Hatziargyriou, “An Enhanced IEEE 33 Bus Benchmark Test System for Distribution System Studies”, *IEEE Trans. Power Syst.*, vol. 36, pp. 2565-2572, 2021.